Modelling W/O/W double emulsions preparation in static mixers: accounting for the shear-thinning behaviour of the dispersed phase

Noureddine Lebaz, Kristy Touma, Ranim Chakleh, Fouad Azizi, Nida Sheibat-Othman

Modelling W/O/W double emulsions preparation in static mixers: accounting for the shear-thinning behaviour of the dispersed phase

Noureddine Lebaz[1*]; Kristy Touma[1]; Ranim Chakleh[1]; Fouad Azizi[2]; Nida Sheibat-Othman[1]

[1] Universite Claude Bernard Lyon 1, CNRS, LAGEPP UMR 5007, F-69100, Villeurbanne, France

[2] B.&W. Bassatne Department of Chemical Engineering and Advanced Energy, American University of Beirut, PO Box 11-0236, Riyad El-Solh, Beirut, Lebanon

1 Abstract

The dispersion of a shear-thinning non-Newtonian fluid using in-line mixers to prepare double emulsions is investigated experimentally and numerically in this study. A two-step method is adopted for the preparation of double emulsions, comprising in a first step the preparation of a reverse water-in-oil (W/O) emulsion using a high-shear rotor-stator device. This inner emulsion is dispersed in a second step into an outer aqueous phase by continuous parallel pumping of both phases through a set of static mixers. The second preparation step is modelled using a population balance equation (PBE) accounting for droplet breakage inside the mixers. Since the inner emulsion behaves as a shear-thinning fluid, the breakage efficiency depends on the local shear rate. Using classical turbulent breakage kernels is therefore inappropriate, hence there is a need for a kernel accounting for the shear-thinning character of the dispersed phase. To tackle this issue, single-phase CFD simulations of the fluid flow through the mixers are carried out showing a high shear rate magnitude near the walls of the pipe and the mixer crossbars. To avoid CFD-PBE direct coupling, the probability density function (PDF) of the shear rate is extracted from the CFD simulations. This PDF is then used to develop a volume-averaged PBE, where a classical Ostwald-de Waele model is

[*] Corresponding author. Address : LAGEPP, Université Claude Bernard Lyon 1, bât 308G ESCPE-Lyon, 43 bd du 11 Novembre 1918, Villeurbanne 69622 France. Tel.: +33 04 72 43 18 55; Fax: +33 04 72 43 16 99
Email address: noureddine.lebaz@univ-lyon1.fr (Noureddine Lebaz)

employed to relate the apparent viscosity of the inner emulsion to the shear rate. Different experimental parameters influencing the quality of the dispersion are investigated, including the fraction of the inner emulsion phase, the oil viscosity and the inner and outer aqueous phase viscosities. In the different cases, the model captures the transient evolution of the droplet size distribution of the W/O/W double emulsions at the outlet of the mixers while the computational time remains very low.

Keywords: Double emulsions, static mixers, droplet breakage, shear-thinning fluids, population balance model, probability density function of shear rate.

2 Introduction

Liquid-liquid dispersions are commonly encountered in many applications including food, pharmaceutical, agricultural, and petrochemical industries (Bibette et al., 1999). The whole properties of these multiphase systems, referred to as emulsions rely on the dispersion quality in terms of the droplet size distribution (DSD). Practically, the dispersing unit, the operating conditions, and the physicochemical properties and concentrations of the constitutive ingredients contribute to the final preparation attributes (Piorkowski and McClements, 2014).

The complexity of liquid-liquid systems increases regarding quality control when considering multiple emulsions. In the case of double emulsions, the preparation is commonly achieved in two successive steps (Ding et al., 2019). In the first step, a fine emulsion is obtained using high-shear devices (Muschiolik and Dickinson, 2017). In the second step, the inner emulsion obtained in the first step is dispersed in a continuous phase using moderate shear devices to form the outer droplets. To stabilize the system, at least, two surfactants are employed and dissolved in the intermediate and the outer phases. This formulation process is, for instance, adopted for the encapsulation of pharmaceutical active ingredients to provide their controlled release (Fabiilli et al., 2010). Since one of the objectives of double emulsion systems is achieving a high encapsulation efficiency, the inner emulsion is usually concentrated. However, increasing the dispersed phase fraction strongly impacts the rheological behaviour of the emulsion (Pal, 2006). Mixtures of non-miscible Newtonian fluids with fractions more than 5 wt.% show a shear-thinning behaviour that is also sensitive to the droplet size distribution (Pal, 1996).

Several experimental and numerical studies investigated the impact of various operational conditions on the quality of turbulent liquid-liquid dispersions. These parameters ranged from

the dispersed phase viscosity (Calabrese et al., 1986; Hert and Rodgers, 2018), to continuous phase viscosity (Hert and Rodgers, 2019; Lebaz and Sheibat-Othman, 2022), dispersed phase volume fraction (Becker et al., 2011; Lobry et al., 2011), energy dissipation (Buffo et al., 2016; Zainal Abidin et al., 2014), surfactant type (Li et al., 2017; Skelland and Moeti, 1989) and other similarly relevant parameters. However, only a few modelling studies were devoted to the emulsification of non-Newtonian fluids even though these fluids are omnipresent in the food engineering and pharmaceutical applications. For instance, shear-thinning droplet formation mechanisms were studied in small-scale devices, such as capillary tubes and microchannels (Davidson and Cooper-White, 2006; Liu et al., 2022; Wong et al., 2019). Multiphase Computational Fluid Dynamics (CFD) can also be used for tracking single drop formation in microchannels (Wong et al., 2017).

The population balance equation (PBE) is now a well-established framework for modelling dispersed systems including emulsions, bubbly flows, crystallization and precipitation operations (Ramkrishna and Singh, 2014). Extensive research has been reported on modelling turbulent liquid-liquid dispersions in stirred tanks (Gao et al., 2016), high-shear rotor-stator mixers (Michael et al., 2017), high-pressure homogenizers (Bagkeris et al., 2019) and static mixers (Lebaz and Sheibat-Othman, 2019a). In the case of the double emulsions, (Khadem and Sheibat-Othman, 2019a) developed a population balance model for the prediction of the outer droplet size distribution and inner droplet leakage during the preparation process using a high-shear rotor-stator device. A correlation of the outer droplet viscosity was considered to correct for the fraction of the inner emulsion, but the dispersion was considered as a Newtonian fluid.

Recently, an original process based on the use of a combination of a high-shear device for the preparation of the inner emulsion and a continuous process of static mixers for the second step of emulsification was demonstrated to be efficient for the preparation of water-in-oil-in-water (W/O/W) double emulsions (Lebaz et al., 2023). This study pointed out the non-Newtonian behaviour of the inner emulsion. The shear-thinning character was found to be strongly dependent on the inner phase fraction, and less on the inner phase viscosity or droplet size. Regarding the second emulsification step, static mixers allowed monomodal DSDs under the different investigated conditions with a high encapsulation efficiency, since the preparation time (residence time inside the static mixers) took less than one second.

In this study, a specific focus is set on modelling the second emulsification step, following a population balance approach, to predict the outer DSD of W/O/W emulsions at the outlet of

the static mixers. The originality of the developed model is the consideration of the shear-thinning behaviour of the inner emulsion which means that droplet breakage will be dependent on the local shear rate inside the mixers. It is worth noting that droplet coalescence is negligible in our case because of the low dispersed phase fraction and the use of a stabilizer. To do so, single-phase CFD simulations are conducted to access the flow properties throughout the static mixers. To avoid direct CFD-PBE coupling which is computationally intensive, a volume-average model is formulated by considering a spatial distribution of the shear rate for which the probability density function (PDF) is extracted from the CFD simulations. This allows us to accurately capture the interaction between the dispersed and continuous phases with a very low computational cost. Several operating conditions are varied to identify the model parameters and validate its prediction quality.

3 Materials and experimental methods

3.1 Materials

The W/O/W double emulsions are prepared using ultrapure water (Synergy unit system, Millipore, France) and silicone oils of different viscosities as reported in Table 1 (provided by Sigma-Aldrich, Germany). As stabilisers, two surfactants are employed: Abil® EM97S (offered by Evonik, Germany) dissolved in the oil phase and Polysorbate 20 (Tween®20, Sigma-Aldrich, Germany) dissolved in the outer aqueous phase. For osmotic pressure regulation, sodium chloride (Sigma-Aldrich, Germany) is dissolved in the internal aqueous phase. Glycerol (VWR Chemicals, France) is used as a viscosity enhancer of the aqueous phases. All chemicals used are of analytical grade and are used as received without further purification.

3.2 Double emulsion preparation and characterization

The procedure adopted for the preparation of the double emulsions is schematically summarized in Figure 1, following a classical two-step method. First, a reverse W/O emulsion is prepared by mixing silicone oil, containing 2 wt. % of the lipophilic surfactant Abil EM97S, with an aqueous phase, in which sodium chloride is previously dissolved at a concentration of 0.1 M. Since a fine emulsion is intended, a high-shear rotor-stator device (IKA T 18 digital ULTRA-TURRAX®) is used for 4 min at 12000 rpm in all the preparations. Dynamic light scattering (Malvern Zetasizer Nano ZS®) is used for DSD measurements after significant dilution in silicone oil. The rheological behaviour of the inner emulsions is

assessed using an MCR 302 rheometer (Anton Paar, France) equipped with a 25 mm cone-plate geometry under a shear rate ranging from 0 to 1000 s^{-1}. It is worth noticing that all the individual phases are Newtonian fluids. Besides, the inner W/O emulsions remain stable for several days due to their high viscosity (limiting droplet diffusion and collision), the use of emulsifier, and the low solubility of water in oil (limiting Ostwald ripening). DSD measurements were carried out (by DLS) before and after shearing, leading to identical measurements, so indicating that there was no impact of shearing on the DSD under these conditions. Second, the prepared (inner) emulsion in the first step is pumped in parallel with the aqueous phase (containing 2 $g.L^{-1}$ of Tween®20) through a set of static mixers (using MCP-Z Ismatec gear pumps) at a constant dispersed fraction of 1 wt. %. Because of the significant difference between the flow rate of the two phases, a needle is used to introduce the dispersed phase in parallel to the tube (of 5 mm) where the continuous phase circulates. The internal diameter of the needle is sufficiently bigger than the water droplets to avoid modifying the inner emulsion properties. A total of twenty SMX+ (Sulzer) elements were mounted inside the tube, each being rotated by 90° with respect to the previous one to minimize preferential fluid flow pathways. The technical characteristics of these mixers are summarized in (Lebaz and Sheibat-Othman, 2019b).

A pressure gauge (Keller LEO1: 0–3 bar, ± 3 mbar, Germany) was installed upstream of the static mixers for pressure drop measurement during the emulsification process. For each experiment, two samples were withdrawn for DSD and conductivity measurements: after 5 and 20 mixing elements. The DSD of the prepared W/O/W double emulsions was measured offline using laser diffraction (Mastersizer 3000, Malvern Instruments, France) after significant dilution in water. The measurements were repeated 3 times to minimize the uncertainties on the DSD. The interfacial tension (σ) between the inner emulsion and the outer aqueous phase was obtained by a Drop Shape Analysis System DSA10 Mk2 (Krüss GmbH, Germany) based on the pendant drop method. The encapsulation efficiency was directly related to the released amount of salt during the emulsification process (second step) and was therefore monitored by electrical conductivity measurement using a Transmitter M200 probe (Mettler-Toledo). Table 1 summarizes the different physicochemical and operating parameters varied during the W/O/W double emulsions preparation.

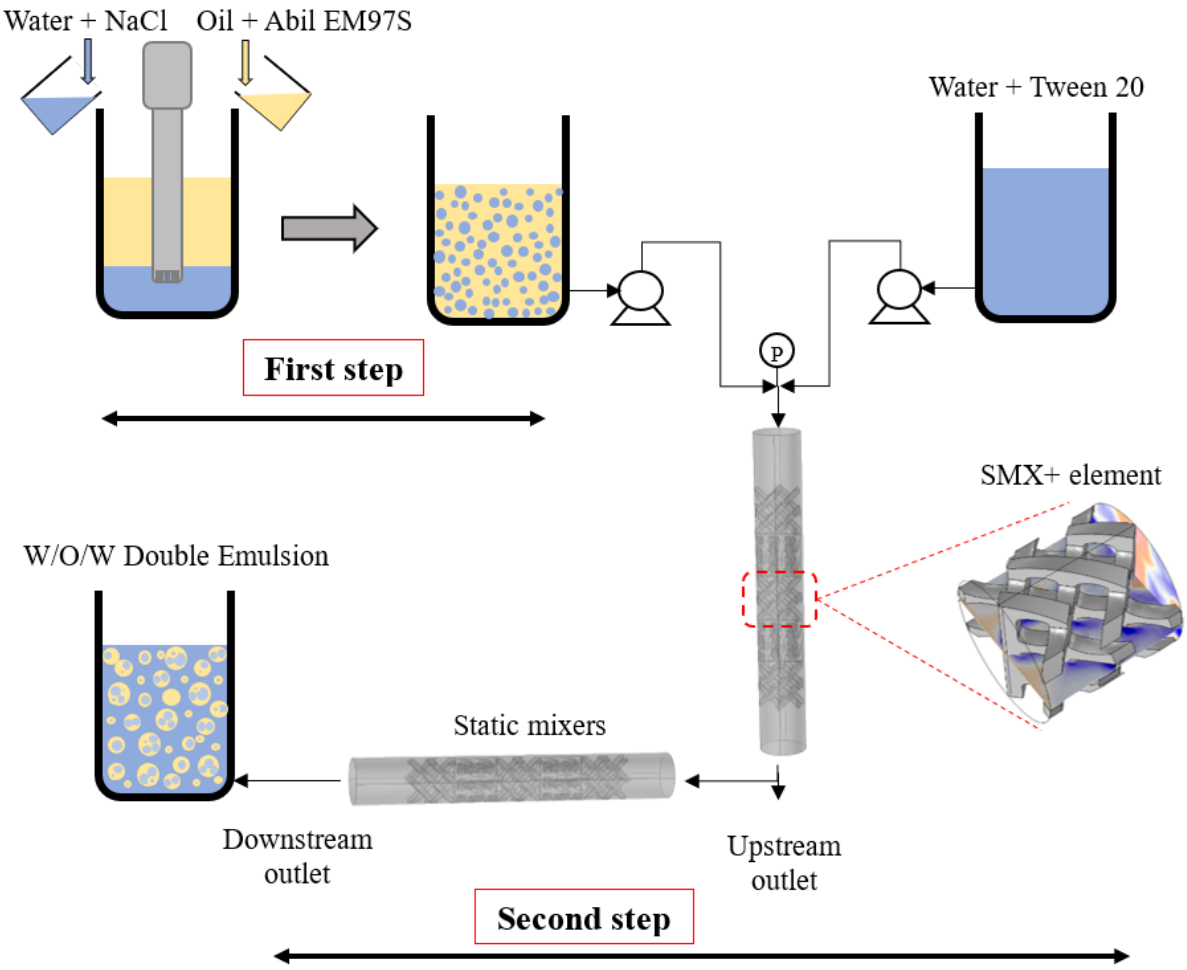

Figure 1: Experimental set-up for the preparation of W/O/W double emulsions using a two-step method based on a high-shear device (Ultra-Turrax) and SMX+ static mixers.

Table 1: List of experiments carried out for the preparation of the W/O/W double emulsions.

Case n°	μ_{wi} [mPa s]	μ_o [mPa s]	μ_c [mPa s]	ϕ_i [wt. %]	Re_h [-]	$\bar{\varepsilon}$ [m^2 s^{-3}]	σ [mN m^{-1}]
1	1	5	1	40	1000	237	6
2	1	10	1	40	1000	237	6
3	1	20	1	40	1000	237	6
4	1	100	1	40	1000	237	6
5	5	5	1	40	1000	237	6
6	5	10	1	40	1000	237	6
7	5	20	1	40	1000	237	6
8	5	100	1	40	1000	237	6
9	10	5	1	40	1000	237	6
10	10	10	1	40	1000	237	6
11	10	20	1	40	1000	237	6
12	10	100	1	40	1000	237	6
13	20	5	1	40	1000	237	6
14	20	10	1	40	1000	237	6
15	20	20	1	40	1000	237	6
16	1	10	5	40	300	665	2

17	1	10	10	40	300	3963	1.5
18	1	10	1	30	1000	237	6
19	1	10	1	20	1000	237	6
20	1	10	1	10	1000	237	6

To ensure turbulent emulsification, the hydraulic Reynolds number ($\mathrm{Re_h}$), given by the following equation, is kept higher than 260 in all the cases (Theron and Le Sauze, 2011) :

$$\mathrm{Re_h} = \frac{\rho_c u_s D_h}{\varphi \mu_c} \quad (1)$$

Where ρ_c and μ_c are the density and the dynamic viscosity of the continuous phase respectively, u_s is the superficial velocity, D_h is the hydraulic diameter of the pipe equipped with the static mixers and φ is the global porosity of the mixers.

4 Theoretical framework

4.1 CFD simulations

The hydrodynamics of flows through SMX+ mixers were previously investigated in our earlier study (Azizi et al., 2022), where turbulent single-phase flows passing through a series of mixing elements were simulated, and the impact of varying the velocity and viscosity of the flow on the velocity field, extensional efficiency, helicity, and turbulence were reported. The results showed that at a constant $\mathrm{Re_h}$, the viscosity had no noticeable effect on these parameters as opposed to the flow velocity. The analysis revealed that both the radial and tangential components of the velocity vector are of considerable magnitude inside the mixer, so the flow cannot be considered as one-dimensional. The strain rate distribution within the mixer was found to be non-uniform, with its peak values situated at the solid walls of either the pipe or the mixer crossbars, thereby corroborating the findings of (Liu et al., 2006).

The simulations also showed that the majority of the stretching and elongation of fluid elements occur in the first part of the mixing element where the extensional efficiency is highest, indicating good dispersive behavior. Nonetheless, various parameters and average values become constant beyond the second mixer. The presence of consecutively rotated mixers induced a rotational flow downstream of the final mixer. In this region, a central core of spiralling flow, coupled with a near-wall region characterized by fluid elements whirling orthogonal to the flow direction, was observed. For more detailed information on the CFD simulation and analysis of the flow, the reader is referred to our earlier work (Azizi et al.,

2022). It should be noted that the single-phase simulations were performed using a constant apparent viscosity of the mixture consistent with our previous population balance work (Lebaz et al., 2022).

4.2 Modelling droplet breakage in static mixers

In the double emulsification process, the first step consists of the preparation of a single reverse emulsion using a high-shear device (Ultra-Turrax). Modelling single emulsions is widely addressed in the literature, hence it will not be considered in this study (Gallassi et al., 2019; Li et al., 2022). The modelling task here will focus on the second step dealing with the dispersion of the inner reverse emulsion into the outer aqueous phase within static mixers to form the double emulsion (DE). The few available studies in the literature on the modelling of DE preparation employed different processes than static mixers. These investigations proposed correlations for either the release rate of the inner droplets (Klahn et al., 2002; Okazaki et al., 1992) or the prediction of the outer droplets mean diameter (Gallego-Lizon and Pérez de Ortiz, 2000; Khadem and Sheibat-Othman, 2019b).

The second step of double emulsification may be viewed as a single emulsification in which the dispersed phase is a fine emulsion (Schuch et al., 2013). As a continuity of our recent works on modelling single emulsification using static mixers (Lebaz et al., 2022; Lebaz and Sheibat-Othman, 2022), a population balance equation is used to describe the evolution of the outer droplet size distribution during their residence time within the static mixers, where only breakage is considered (equation 2).

$$\frac{\partial n(\boldsymbol{x},v,t)}{\partial t} = \int_v^\infty b(v,v')g(\boldsymbol{x},v')n(\boldsymbol{x},v',t)\mathrm{d}v' - g(\boldsymbol{x},v)n(\boldsymbol{x},v,t) \qquad (2)$$

where $n(\boldsymbol{x},v,t)$ is the number-based DSD density at position $\boldsymbol{x}$ and time t, v is the droplet volume, $g(\boldsymbol{x},v)$ is the breakage kernel of a droplet of size v, and $b(v,v')$ is a function describing the volume distribution of daughter droplets generated by the breakage of a droplet of volume v'. The first term on the right-hand side accounts for the birth of droplets of volume v resulting from the breakage of bigger droplets of volume v', and the last term is the death term due to the loss of droplets of volume v because of their breakage.

The choice of droplet breakage as the unique mechanism occurring within the static mixers is justified by the low dispersed phase fraction of the second emulsion (1 wt. %) and the use of a hydrophilic surfactant with a concentration higher than its critical micellar concentration which makes droplet coalescence negligible (Raikar et al., 2009). Moreover, because of the

low solubility of silicone oils in water, Ostwald ripening is negligible. Finally, one of the interesting features of static mixers is the uniform spatial distribution of turbulence intensity unlike in rotor-stator devices or classical stirred tanks (Azizi et al., 2022). This allows the formulation of the population balance equation without the convective term as the dispersion is spatially uniform. However, the shear rate is not uniformly distributed, as it will be highlighted later. And, as recently reported for W/O/W double emulsions, the inner emulsion is non-Newtonian showing a strong shear-thinning behaviour (Lebaz et al., 2023). This is mainly due to the high internal aqueous phase fraction ranging from 10 to 40 wt. %. The viscosity of the inner emulsion, and therefore their breakage, $g(\boldsymbol{x}, v)$, will depend on the local shear rate. Therefore, we need to relate the breakage kernel to the local shear rate in the static mixers. In the current study, to avoid direct coupling between CFD and PBE, a 0D volume-averaged PBE combined with the probability density function (PDF) of the shear rate is developed, in analogy to the work by (Buffo et al., 2016) for the PDF of energy dissipation rate.

Assuming a uniformly distributed number density, the volume-averaged density of droplets can be obtained by:

$$\bar{n}(v,t) = \frac{1}{V}\int_V n(\boldsymbol{x}, v, t)\mathrm{d}\boldsymbol{x} \tag{3}$$

where V is the volume of fluid in the mixers. So, equation 2 becomes:

$$\frac{\partial \bar{n}(v,t)}{\partial t} = \int_v^\infty b(v, v')\bar{n}(v', t)\frac{1}{V}\int_{\boldsymbol{x}} g(\boldsymbol{x}, v')\mathrm{d}\boldsymbol{x}\,\mathrm{d}v' - \bar{n}(v,t)\frac{1}{V}\int_{\boldsymbol{x}} g(\boldsymbol{x}, v)\mathrm{d}\boldsymbol{x} \tag{4}$$

The only spatial dependency is therefore related to the breakage kernel. To consider the dependence of droplet breakage on the local shear rate, and since the dispersed phase is non-Newtonian, a volume-average kernel is formulated as follows:

$$\bar{g}(v) = \frac{1}{V}\int_V g(\boldsymbol{x}, v)\mathrm{d}\boldsymbol{x} = \int_0^\infty g(\dot{\gamma}, v) f(\dot{\gamma})\mathrm{d}\dot{\gamma} \tag{5}$$

where $\dot{\gamma}$ is the shear rate and $f(\dot{\gamma})$ is the PDF of the shear-rate in the mixers, so that $f(\dot{\gamma})\mathrm{d}\dot{\gamma}$ represents the fluid volume fraction experiencing a shear rate between $\dot{\gamma}$ and $\dot{\gamma} + d\dot{\gamma}$.

The dispersed phase is considered a shear-thinning pseudo-single-phase system with an apparent viscosity μ_d. The latter is modelled using the Ostwald-de Waele (power law) model with a maximum at low shear rates and a plateau at high shear rates (Meriem-Benziane et al., 2012; Rosti and Takagi, 2021):

$$\mu_{\mathrm{d}} = K\dot{\gamma}^{m-1} \tag{6}$$

where K is the consistency coefficient and m is the fluid flow index. These two parameters are identified from experimental data fitting. Other viscosity models such as the Herschel-Bulkley model and the Carreau model are also commonly used, but they require knowing the viscosity at zero and infinite shear stresses, contrary to the Ostwald-de Waele model (Dubbelboer et al., 2016; Ferrari et al., 2023).

4.3 Breakage kernel and daughter size distribution

One of the most popular breakage kernels for liquid-liquid systems is that developed by (Coulaloglou and Tavlarides, 1977). In the classical phenomenological Coulaloglou and Tavlarides model framework, the droplet breakage is assumed to be effective if the disruptive turbulent energy of eddies is higher than the cohesive energy due to surface tension. It was later proven that the viscous force of the dispersed phase contributes to the cohesion of the droplets to be then integrated into the breakage probability (Chen et al., 1998). Another basis of the Coulaloglou and Tavlarides model is the assumption of breakage events occurring exclusively within the inertial subrange of isotropic turbulence. However, it was recently demonstrated that during emulsification in SMX+ static mixers, droplet breakage occurs within the inertial and dissipative subranges of turbulence, and a kernel considering the full spectrum of turbulence was employed (Lebaz et al., 2022):

$$g(d,\dot{\gamma}) = \frac{C_1\sqrt{\overline{u^2}(d)}}{d}\exp\left(-\frac{C_2\sigma}{\rho_{\mathrm{d}}\, d\, \overline{u^2}(d)} - \frac{C_3\mu_{\mathrm{d}}(\dot{\gamma})}{\rho_{\mathrm{d}}^{3/2}\rho_{\mathrm{c}}^{-1/2}\, d\sqrt{\overline{u^2}(d)}}\right) \tag{7}$$

where d is the droplet diameter, $\bar{u}$ is the mean velocity of a turbulent eddy, σ the surface tension, ρ_{d} and ρ_{c} are the densities of the dispersed and continuous phases respectively, and C_1, C_2, and C_3 are adjustable parameters. The mean fluctuating eddy velocity $\overline{u^2}(\lambda)$ may be approximated by the second-order longitudinal structure function $\langle[\delta u]^2\rangle(\lambda)$ (Karimi and Andersson, 2018), for which a semi-empirical formula is proposed for the inertial and dissipation subranges (Kolmogorov, 1941; Sawford and Hunt, 1986):

$$\langle[\delta u]^2\rangle(\lambda) = C(\varepsilon\lambda)^{2/3}\left(\frac{\lambda^2}{\lambda_{\mathrm{d}}^2+\lambda^2}\right)^{2/3} \tag{8}$$

where C is the Kolmogorov constant, λ is the eddy size, ε is the turbulent energy dissipation rate and λ_{d} is a length scale relation (equation 9) proportional to the Kolmogorov length scale η (equation 10).

$$\lambda_{\mathrm{d}} = (15C)^{3/4}\eta \tag{9}$$

$$\eta = \left(\frac{{\upsilon_{\mathrm{c}}}^3}{\varepsilon}\right)^{1/4} \tag{10}$$

where υ_{c} is the kinematic viscosity of the continuous phase. In our specific case, the mean turbulent energy dissipation rate $\bar{\varepsilon}$ is accessible experimentally through the measurement of the pressure drop induced by the static mixers:

$$\bar{\varepsilon} = \frac{\Delta P u_{\mathrm{i}}}{\rho_{\mathrm{c}} L_{\mathrm{s}}} \tag{11}$$

where L_{s} is the total length of the static mixing elements and u_{i} is the interstitial velocity estimated as:

$$u_{\mathrm{i}} = \frac{u_{\mathrm{s}}}{\varphi} = \frac{4Q}{\pi D_s^2}\frac{1}{\varphi} \tag{12}$$

where Q is the volume flow rate of the fluid and D_{s} is the internal diameter of the tube.

Regarding the daughter size distribution function, the beta function is adopted, which assumes a binary breakage with the highest probability for symmetric events (Hsia and Tavlarides, 1983; Laakkonen et al., 2006):

$$b(v, v') = \frac{60}{v'}\left(\frac{v}{v'}\right)^2\left(1 - \frac{v}{v'}\right)^2 \tag{13}$$

4.4 Numerical aspects

The population balance equation (equation 2) was solved numerically using the finite volume method initially proposed by (Filbet and Laurençot, 2004) for the coagulation equation and later extended by (Kumar et al., 2009) for breakage processes. The spatial axis was divided into 100 bins with a geometrical progression, following the Mastersizer grid measurements. The identification of the parameters appearing in the breakage kernel (equation 7) was carried out by minimizing the absolute difference between the experimental volume-based DSD histogram and the corresponding model predictions. To do so, the least-square non-linear solver *lsqnonlin* (Matlab®) was used over the total set of experiments reported in Table 1.

5 Results and discussion

5.1 Rheology of the inner emulsions

As reported in the literature and our recent work, the rheology of emulsions is importantly affected by the dispersed phase fraction and can be affected by its DSD (Lebaz et al., 2023; Pal, 2006, 1996). In our case, the prepared inner W/O emulsions show an increasing shear-thinning behaviour as the dispersed aqueous phase fraction increases (Figure 2-left). Also, increasing the inner water phase increases the viscosity significantly. It is worth noting that in this case, the inner DSD remained the same since the different phase fractions were obtained by dilution of a concentrated emulsion of $\phi_i = 40\ wt.\%$. Thus, the difference in the apparent viscosity of the inner emulsion shown in Figure 2-left is only due to the difference in phase fraction.

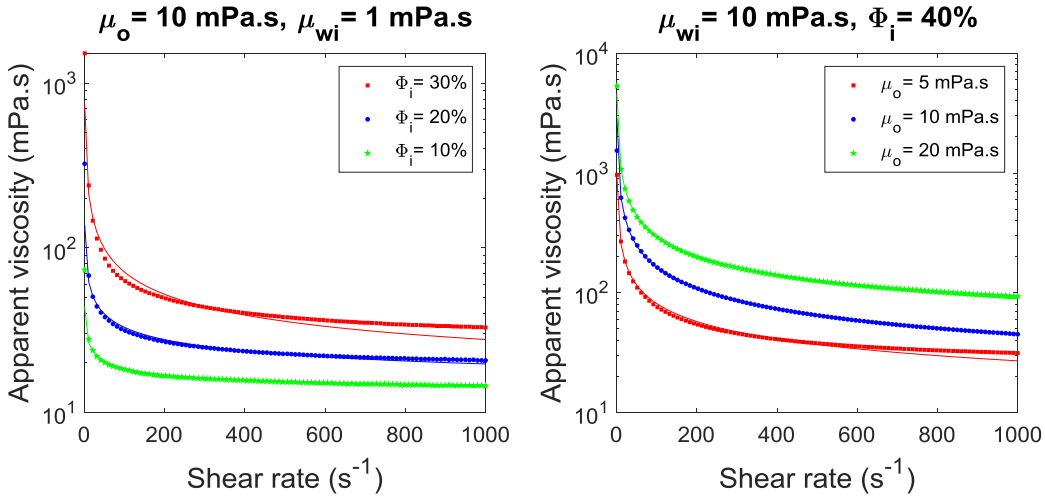

Figure 2: Apparent viscosity of the inner emulsion as a function of the shear rate under different conditions. The symbols refer to the experimental data and the continuous lines to the shear-thinning viscosity model (equation 6).

As expected, increasing the continuous phase viscosity of the inner reverse emulsion (i.e. oil) shifts the rheological behaviour towards higher viscosities as shown in Figure 2-right. In this case, the inner DSDs are slightly different but this parameter (as well as the inner aqueous phase viscosity) was not significantly influencing the apparent viscosity of the emulsions as reported by (Lebaz et al., 2023). In the different cases shown in Figure 2, the shear-thinning Ostwald-de Waele model (equation 6) gives a very good fit of the apparent viscosity of the emulsions as a function of the shear rate. The two parameters (K and m) of the Ostwald-de Waele model are fitted for each experiment separately and the result is implemented in the

breakage kernel where an accurate estimation of the viscosity of the dispersed phase at any given shear rate can be obtained. The fitted parameters are within the intervals $K \in [3.4\,,283]$ and $m \in [-0.64\,,-0.30]$.

5.2 Shear rate distribution

As fluid elements pass through the static mixers, they are progressively sheared due to the development of the shear stress field. The shear rate magnitude, $|\langle S\rangle|$, can be computed using equation 14, which relies on the magnitude of the shear rate tensor, $\langle S\rangle$, (shown in equation 15). The components of the latter are functions of the mean velocity field following Reynolds averaging for the turbulent flow field.

$$|\langle S\rangle| = \sqrt{2\langle S\rangle : \langle S\rangle} \tag{14}$$

$$\langle S\rangle = \frac{1}{2}\left(\nabla\langle\vec{U}\rangle + \left(\nabla\langle\vec{U}\rangle\right)^{T}\right) \tag{15}$$

where $\langle\vec{U}\rangle$ is the mean velocity component of the instantaneous velocity $\vec{U}$. The simulations were done for the three cases (15, 16 and 17) reported in Table 1 for which the viscosity of the continuous phase was varied.

Figure 3 shows the contour plots of the strain rate magnitude at various locations within the second mixer in the series. The results are reported at various dimensionless lengths, L^*, whereby a value of $L^* = 0$ corresponds to the inlet of the mixing element, while $L^* = 1$ indicates the outlet of the same element. As can be observed, and regardless of the variations in the viscosity, density, and average velocity, the shear rate magnitude is always highest near the walls of the pipe and the mixer crossbars. This is expected since the highest velocity gradients exist in these regions.

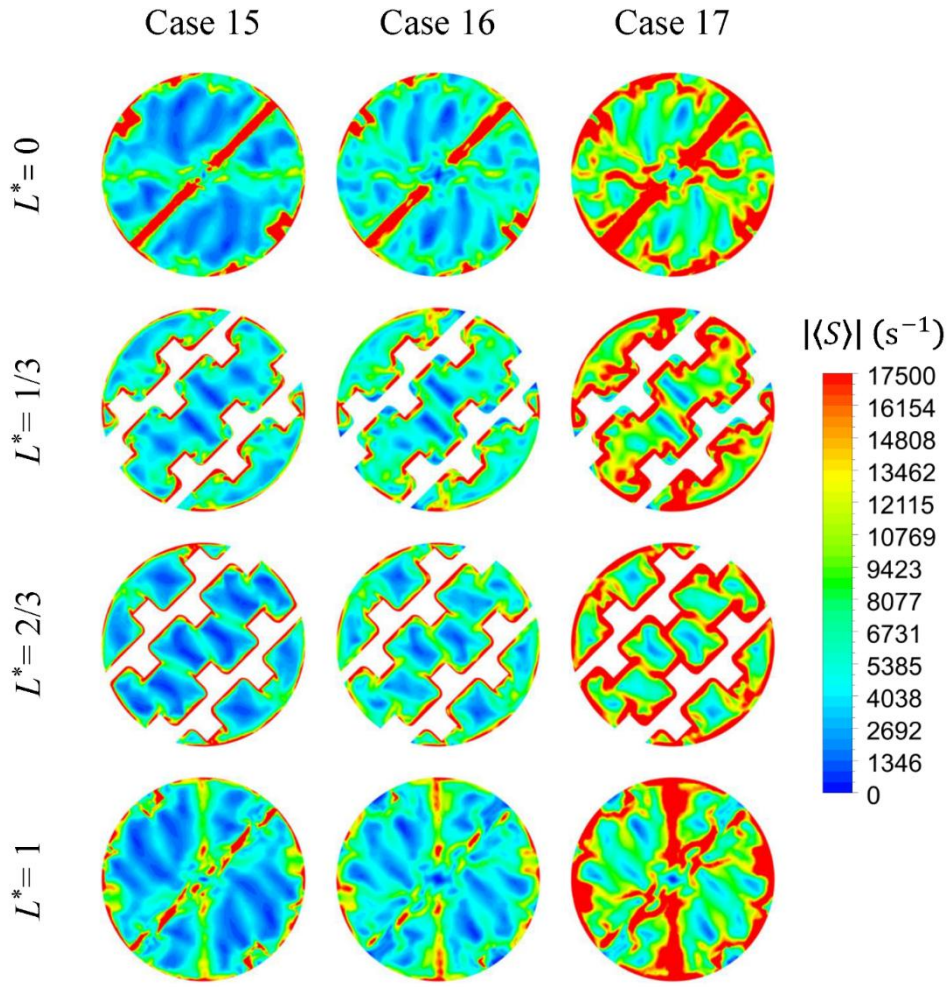

Figure 3: Contour plots of the shear rate magnitude at various locations within the 2nd mixing element for cases 15, 16 and 17.

To quantify the shear rate distribution within the mixer volume and to better evaluate how it is affected by the flow conditions, the PDF of the shear rate magnitude within the 3rd mixing element was extracted from the CFD simulations. A set of 400 sample points representing the distribution of the shear rate magnitude for each element was used. These ensured that 99 % of the total number of cells within the mixer volume were accounted for. Figure 4a shows the shear rate PDF in the third mixer for the various cases as a function of the shear rate magnitude. It can be clearly observed that the PDF for all cases resembles a log-normal distribution with the length of its tail being dependent on the operating conditions. Increasing the fluid viscosity while maintaining comparable velocities (compare cases 15 and 16) results in similar PDFs, albeit with a lower peak for the higher viscosity, which indicates that varying the viscosity did not impact the distribution of the shear rate. However, changing the velocity

of the flow while maintaining the same ratio of inertial to viscous forces, i.e., the same Re_h (compare cases 16 and 17), had a more pronounced impact on the shear rate distribution. Figure 4a clearly shows that case 17 (i.e., higher flow velocity), spans a larger range of shear rates and consequently, the fluid elements can be subjected to higher shearing as they pass through the mixer. This is also obvious in Figure 4b which plots the normalized PDF against the shear rate magnitude within the same mixer. Cases 15 and 16 resulted in almost identical probability density functions, while case 17 shows a much broader span over larger values of the shear rate magnitude.

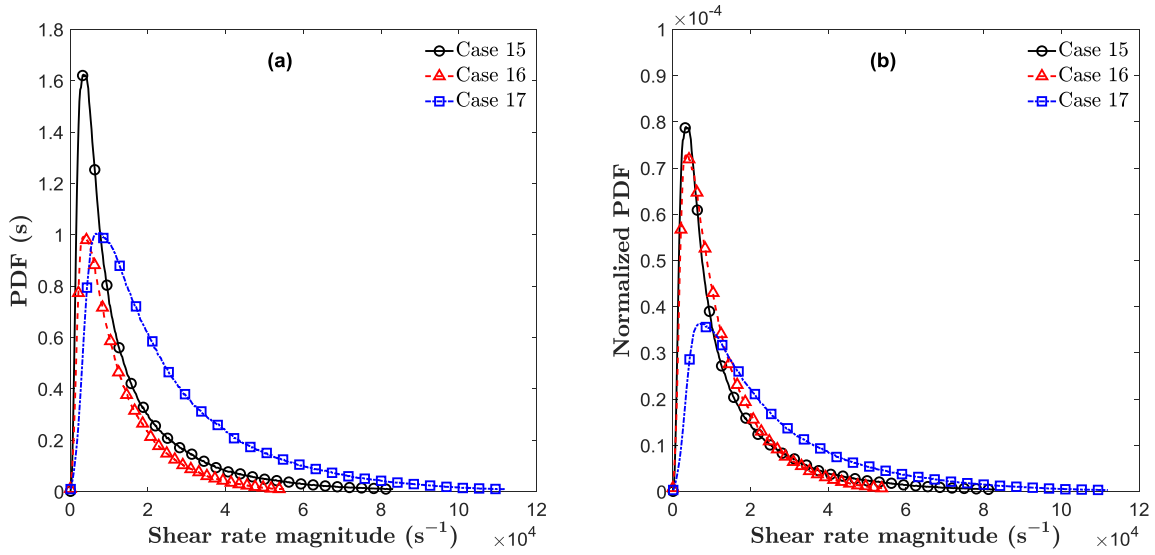

Figure 4: (a) PDF of the shear rate magnitude for the various cases within the third mixing element; (b) Normalized PDF of the shear rate magnitude within the same element.

5.3 Model identification and predictions of the outer DSD

The model parameters appearing in the modified Coulaloglou and Tavlarides breakage kernel were identified using the entire set of the available experimental data depicted in Table 1. A global optimization method was adopted by starting from various initial points to avoid convergence toward local minima. The results are given in Table 2.

Table 2: Identified breakage kernel parameters using all the available experimental data (Table 1)

C_1	C_2	C_3
5.8×10^{-3}	3.30	0.37

For liquid-liquid single emulsification in stirred tanks, the pre-exponential factor is generally set equal to $C_1 = 4.8 \times 10^{-3}$ which is nearly the same as that identified by (Li et al., 2017). Regarding the two other constants, there is no consensus in the literature since different formulations of the breakage kernel (with only surface stresses in the original kernel, with/without extension to the dissipation subrange of turbulence, … etc.) and different systems/devices are investigated.

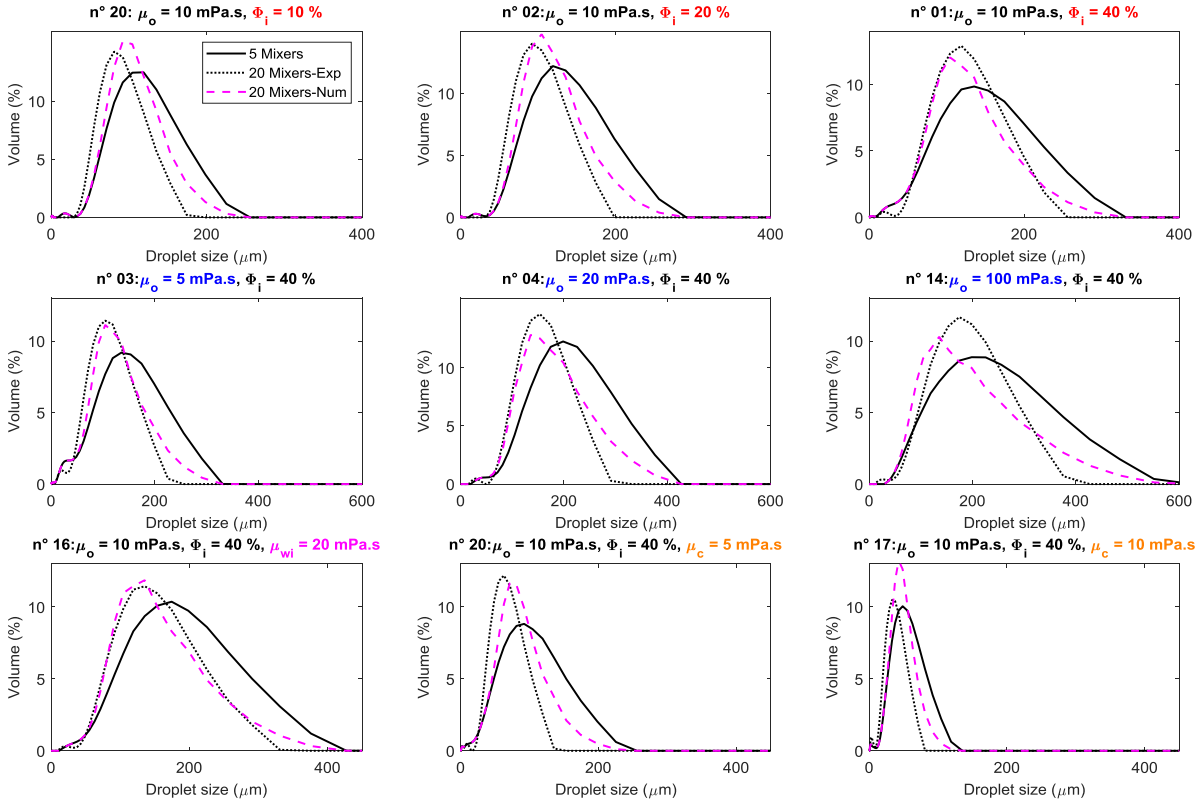

Figure 5: Comparison of the predicted and experimental DSDs of the W/O/W double emulsions at the outlet of the static mixers obtained in different conditions (variation of the inner aqueous phase fraction and viscosity, the oil viscosity and the outer aqueous phase viscosity). The subplot number (n°) refers to the case number in Table 1.

Regarding the model predictions, Figure 5 gives a comparison between the experimental volume-based DSD and that predicted by the PBE when varying different parameters such as the inner aqueous phase fraction and the viscosity of the three different phases. It can be seen that despite the shear-thinning character of the dispersed phase and the large interval of variation of the investigated parameters, the model captures in most cases the transient evolution of the DSD. The physical interpretation of the model is that, despite the fact that the

viscosity of the inner emulsion might be high at low shear, the droplets might undergo fast breakage because their viscosity decreases radically at high shear rates. The model over-predicts however the outlet droplet sizes when the viscosity of the continuous phase is increased (see the two last subplots). This may be explained by the low number of experiments accounting for this effect (only 2) in the optimization procedure on one side, and the experimental difficulty in measuring with good accuracy the interfacial tension of double emulsions in the presence of glycerol on the other side. In fact, glycerol, used in our case as a viscosity enhancer of the aqueous phase, is known to have a surfactant-like role that might reduce the interfacial tension of the system (Yang and McClements, 2013). This can be seen in Table 1 where the interfacial tension decreases from 6 mN m^{-1} when $\mu_c = 1$ mPa s, to 2 mN m^{-1} when $\mu_c = 5$ mPa s, and to 1.5 mN m^{-1} when $\mu_c = 10$ mPa s. However, the experimental uncertainty on such very low values is high.

When increasing the inner phase fraction (subplots 1-3 in Figure 5), the viscosity of the inner emulsion is increased leading to the shift of the DSD towards bigger sizes. The model slightly overpredicts the experimental DSD for low fractions while the inverse is obtained at high fractions. This may be explained by the fitting quality of the viscosity curves as can be seen in Figure 2, since the shear-thinning behavior increases when increasing ϕ_i. At high fractions, the Ostwald-de Waele model underpredicts the viscosity at high shear, so breakage is enhanced numerically leading to DSD underprediction. Similarly, increasing the oil viscosity (subplots 3-6) enlarges the DSD because of the increasing viscosity of the inner emulsion, and the deviation between the model and the experiments also increases probably for the same reason, or other experimental or modelling uncertainties.

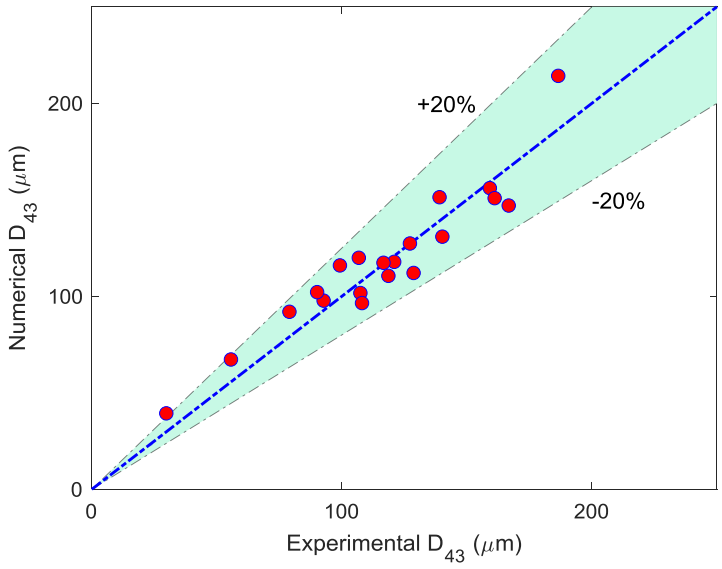

Figure 6: Overall comparison of the predicted volume-based mean diameter (D_{43}) against that obtained experimentally.

To give a more global picture of the model prediction capabilities, Figure 6 compares the predicted volume-based mean diameter (D_{43}) with that obtained experimentally. Despite the large range of variation of the mean diameters (from 30 μm to 190 μm) due to the notably different process and physico-chemical parameters, the predictions remain acceptable.

6 Conclusions

In this study, the emulsification of a shear-thinning non-Newtonian fluid for the production of water-in-oil-in-water (W/O/W) double emulsions is investigated. A classical two-step method is followed for the preparation of double emulsions in which a reverse W/O emulsion is first prepared using a high-shear rotor-stator device. In the second step, the reverse emulsion is dispersed in an aqueous phase by continuous mixing inside in-line static mixers. The efficiency of this system to produce W/O/W double emulsions under different conditions was recently reported by (Lebaz et al., 2023). Here, the emphasis is put on modelling the DSD evolution within the static mixers. For this purpose, a population balance model is used to tackle the transient behaviour of the DSD. Since the dispersed fluid is a reverse emulsion with a high inner aqueous phase fraction (from 10 to 40 wt.%), it shows a shear-thinning character with a variable intensity depending on the inner emulsion composition. This shear-thinning behaviour is well reproduced using the Ostwald-de Waele model. Regarding the implementation of the PBE, and while the classical breakage kernels are most usually developed for Newtonian fluids, the extended Coulaloglou and Tavlarides breakage kernel is employed in this study with a shear rate-dependent viscosity (Coulaloglou and Tavlarides, 1977). Single-phase CFD simulations are conducted and the shear rate probability density function (PDF) is extracted. The shear rate profiles demonstrated that the shear rate magnitude is always highest near the walls of the pipe and the mixer crossbars. The initial homogeneous population balance model is hence reformulated as a volume-averaged PBE that accounts for the dependence of the dispersed phase viscosity on the local shear rate.

After a global optimization of the breakage kernel parameters, the model prediction capabilities are tested against experimental data obtained in different cases. The model showed very good predictions with a very low computational demand. This work constitutes

the first contribution to the modelling of shear-thinning non-Newtonian fluids dispersion in static mixers using a volume-averaged population balance model.

7 Nomenclature

$b(v, v')$	Breakage daughter size distribution	m^{-3}
C	Kolmogorov constant (equation 1, $C = 1.62$)	-
C_i	Parameters of the breakage kernel	-
d	Droplet diameter	m
D_h	Hydraulic diameter of the pipe	m
D_s	Diameter of the pipe	m
D_{43}	Volume-based mean droplet size	m
$f(x)$	The probability density function of x	-
$g(v)$	Volume-based breakage frequency	s^{-1}
K	Consistency coefficient	Pa s^{m-1}
L_s	Length of the SMX+ mixer element	m
L^*	Non-dimensional mixer length	-
m	Fluid flow index	-
$n(\boldsymbol{x}, v, t)$	Number-based density	m^{-4}
$\bar{n}(v, t)$	Volume-averaged number density	m^{-4}
ΔP	Pressure drop	Pa
Q	Volumetric flow rate	$m^3 s^{-1}$
Re_h	Hydraulic Reynolds number	-
t	Time	s
$\bar{u}$	Mean velocity in a turbulent eddy	m s^{-1}
$\vec{U}$	Instantaneous velocity vector	m s^{-1}

$\langle \vec{U} \rangle$	Mean velocity vector	m s^{-1}
u_i	Interstitial velocity	m s^{-1}
u_s	Superficial velocity	m s^{-1}
$\langle [\delta u]^2 \rangle$	One-dimensional second-order longitudinal structure function	m^2 s^{-2}
$\langle S \rangle$	Mean rate of strain tensor	s^{-1}
$\lvert \langle S \rangle \rvert$	Magnitude of mean strain rate tensor	s^{-1}
v, v'	Droplet volume	m^3
V	The volume of the fluid in the mixers	m^3

$\dot{\gamma}$	Shear rate	s^{-1}
ε	Energy dissipation rate	m^2 s^{-3}
$\bar{\varepsilon}$	Volume-average turbulent energy dissipation rate	m^2 s^{-3}
η	Kolmogorov length scale	m
λ	Eddy size	m
λ_d	Length scale for the transition from the inertial to the dissipation subrange of turbulence	m
μ_c	Dynamic viscosity of the continuous aqueous phase	Pa s
μ_d	Apparent dynamic viscosity of the inner emulsion (dispersed phase)	Pa s
μ_o	Dynamic viscosity of the oil phase	Pa s
μ_{wi}	Dynamic viscosity of the inner aqueous phase	Pa s
ν_c	Kinematic viscosity of the continuous phase	m^2 s^{-1}
ρ_c	Continuous phase density	kg m^{-3}
ρ_d	Dispersed phase density	kg m^{-3}
σ	Surface tension	N m^{-1}

φ	Global porosity of the static mixers	-
ϕ_i	Internal aqueous phase weight fraction	-

8 Acknowledgement

This work was funded by Institut de Chimie de Lyon (ICL) and Agence Nationale de la Recherche under the grant agreement ANR-22-CE51-0006-01 (DEPMod Project).

9 References

Azizi, F., Abou-Hweij, W., Lebaz, N., Sheibat-Othman, N., 2022. A numerical evaluation of flows through an SMX-Plus mixer. Chemical Engineering Research and Design 178, 382–394. https://doi.org/10.1016/j.cherd.2021.12.030

Bagkeris, I., Michael, V., Prosser, R., Kowalski, A.J., 2019. Simulation of Turbulent Emulsification in a Sonolator Mixer: Interpretation of Drop Breakage Time. Chemical Engineering & Technology 42, 1555–1565. https://doi.org/10.1002/ceat.201800717

Becker, P.J., Puel, F., Henry, R., Sheibat-Othman, N., 2011. Investigation of Discrete Population Balance Models and Breakage Kernels for Dilute Emulsification Systems. Ind. Eng. Chem. Res. 50, 11358–11374. https://doi.org/10.1021/ie2006033

Bibette, J., Calderon, F.L., Poulin, P., 1999. Emulsions: basic principles. Rep. Prog. Phys. 62, 969. https://doi.org/10.1088/0034-4885/62/6/203

Buffo, A., De Bona, J., Vanni, M., Marchisio, D.L., 2016. Simplified volume-averaged models for liquid–liquid dispersions: Correct derivation and comparison with other approaches. Chemical Engineering Science 153, 382–393. https://doi.org/10.1016/j.ces.2016.07.032

Calabrese, R.V., Chang, T.P.K., Dang, P.T., 1986. Drop breakup in turbulent stirred-tank contactors. Part I: Effect of dispersed-phase viscosity. AIChE Journal 32, 657–666.

Chen, Z., Prüss, J., Warnecke, H.-J., 1998. A population balance model for disperse systems: Drop size distribution in emulsion. Chemical Engineering Science 53, 1059–1066. https://doi.org/10.1016/S0009-2509(97)00328-X

Coulaloglou, C.A., Tavlarides, L.L., 1977. Description of interaction processes in agitated liquid-liquid dispersions. Chemical Engineering Science 32, 1289–1297.

Davidson, M.R., Cooper-White, J.J., 2006. Pendant drop formation of shear-thinning and yield stress fluids. Applied Mathematical Modelling 30, 1392–1405. https://doi.org/10.1016/j.apm.2006.03.016

Ding, S., Serra, C.A., Vandamme, T.F., Yu, W., Anton, N., 2019. Double emulsions prepared by two–step emulsification: History, state-of-the-art and perspective. Journal of Controlled Release 295, 31–49. https://doi.org/10.1016/j.jconrel.2018.12.037

Dubbelboer, A., Janssen, J.J.M., Hoogland, H., Zondervan, E., Meuldijk, J., 2016. Pilot-scale production process for high internal phase emulsions: Experimentation and modeling. Chemical Engineering Science 148, 32–43. https://doi.org/10.1016/j.ces.2016.03.014

Fabiilli, M.L., Lee, J.A., Kripfgans, O.D., Carson, P.L., Fowlkes, J.B., 2010. Delivery of Water-Soluble Drugs Using Acoustically Triggered Perfluorocarbon Double Emulsions. Pharm Res 27, 2753–2765. https://doi.org/10.1007/s11095-010-0277-5

Ferrari, M., Boccardo, G., Buffo, A., Vanni, M., Marchisio, D.L., 2023. CFD simulation of a high-shear mixer for food emulsion production. Journal of Food Engineering 358, 111655. https://doi.org/10.1016/j.jfoodeng.2023.111655

Filbet, F., Laurençot, P., 2004. Numerical Simulation of the Smoluchowski Coagulation Equation. SIAM J. Sci. Comput. 25, 2004–2028. https://doi.org/10.1137/S1064827503429132

Gallassi, M., Gonçalves, G.F.N., Botti, T.C., Moura, M.J.B., Carneiro, J.N.E., Carvalho, M.S., 2019. Numerical and experimental evaluation of droplet breakage of O/W emulsions in rotor-stator mixers. Chemical Engineering Science 204, 270–286. https://doi.org/10.1016/j.ces.2019.04.011

Gallego-Lizon, T., Pérez de Ortiz, E.S., 2000. Drop Sizes in Liquid Membrane Dispersions. Ind. Eng. Chem. Res. 39, 5020–5028. https://doi.org/10.1021/ie000016y

Gao, Z., Li, D., Buffo, A., Podgórska, W., Marchisio, D.L., 2016. Simulation of droplet breakage in turbulent liquid–liquid dispersions with CFD-PBM: Comparison of breakage kernels. Chemical Engineering Science 142, 277–288. https://doi.org/10.1016/j.ces.2015.11.040

Hert, S.C.D., Rodgers, T.L., 2019. On the steady-state drop size distribution in stirred vessels. Part II: Effect of continuous phase viscosity. AIChE Journal 65, e16556. https://doi.org/10.1002/aic.16556

Hert, S.C.D., Rodgers, T.L., 2018. On the steady-state drop size distribution in stirred vessels. Part I: Effect of dispersed phase viscosity. AIChE Journal 64, 3293–3302. https://doi.org/10.1002/aic.16171

Hsia, M.A., Tavlarides, L.L., 1983. Simulation analysis of drop breakage, coalescence and micromixing in liquid-liquid stirred tanks. The Chemical Engineering Journal 26, 189–199.

Karimi, M., Andersson, R., 2018. An exploratory study on fluid particles breakup rate models for the entire spectrum of turbulent energy. Chemical Engineering Science 192, 850–863.

Khadem, B., Sheibat-Othman, N., 2019a. Modeling of double emulsions using population balance equations. Chemical Engineering Journal 366, 587–597. https://doi.org/10.1016/j.cej.2019.02.092

Khadem, B., Sheibat-Othman, N., 2019b. Theoretical and Experimental Investigations of Double Emulsion Preparation by Ultrasonication. Ind. Eng. Chem. Res. 58, 8220–8230. https://doi.org/10.1021/acs.iecr.9b00556

Klahn, J.K., Janssen, J.J.M., Vaessen, G.E.J., de Swart, R., Agterof, W.G.M., 2002. On the escape process during phase inversion of an emulsion. Colloids and Surfaces A: Physicochemical and Engineering Aspects 210, 167–181. https://doi.org/10.1016/S0927-7757(02)00376-X

Kolmogorov, A.N., 1941. Dissipation of energy in locally isotropic turbulence, in: Dokl. Akad. Nauk SSSR. pp. 16–18.

Kumar, J., Warnecke, G., Peglow, M., Heinrich, S., 2009. Comparison of numerical methods for solving population balance equations incorporating aggregation and breakage. Powder Technology 189, 218–229.

Laakkonen, M., Alopaeus, V., Aittamaa, J., 2006. Validation of bubble breakage, coalescence and mass transfer models for gas–liquid dispersion in agitated vessel. Chemical Engineering Science, Advances in population balance modelling 61, 218–228. https://doi.org/10.1016/j.ces.2004.11.066

Lebaz, N., Azizi, F., Sheibat-Othman, N., 2022. Modeling Droplet Breakage in Continuous Emulsification Using Static Mixers in the Framework of the Entire Spectrum of

Turbulent Energy. Ind. Eng. Chem. Res. 61, 541–553. https://doi.org/10.1021/acs.iecr.1c03529
Lebaz, N., Sheibat-Othman, N., 2022. Population balance modelling of a continuous static mixer-based emulsification process. Chemical Engineering Research and Design 188, 645–654. https://doi.org/10.1016/j.cherd.2022.10.022
Lebaz, N., Sheibat-Othman, N., 2019a. A population balance model for the prediction of breakage of emulsion droplets in SMX+ static mixers. Chemical Engineering Journal 361, 625–634. https://doi.org/10.1016/j.cej.2018.12.090
Lebaz, N., Sheibat-Othman, N., 2019b. Modeling Emulsification in Static Mixers: Equilibrium Correlations versus Population Balance Equations. Chemical Engineering & Technology 42, 1691–1701. https://doi.org/10.1002/ceat.201900109
Lebaz, N., Touma, K., Sheibat-Othman, N., 2023. An original continuous process for double emulsions preparation using static mixers: Focus on the viscosity. Colloids and Surfaces A: Physicochemical and Engineering Aspects 674, 131984. https://doi.org/10.1016/j.colsurfa.2023.131984
Li, D., Buffo, A., Podgórska, W., Marchisio, D.L., Gao, Z., 2017. Investigation of droplet breakup in liquid–liquid dispersions by CFD–PBM simulations: The influence of the surfactant type. Chinese Journal of Chemical Engineering 25, 1369–1380. https://doi.org/10.1016/j.cjche.2017.01.014
Li, X., Zhao, S., Guo, J., Li, W., Zhang, J., 2022. Novel Rotor-Stator Assembly Promotes the Emulsification Performance in an Inline High-Shear Mixer. Ind. Eng. Chem. Res. 61, 4722–4737. https://doi.org/10.1021/acs.iecr.1c04972
Liu, S., Hrymak, A.N., Wood, P.E., 2006. Design modifications to SMX static mixer for improving mixing. AIChE Journal 52, 150–157. https://doi.org/10.1002/aic.10608
Liu, X., Liu, Z., Jiang, S., Zhu, C., Ma, Y., Fu, T., 2022. Formation of droplets of shear-thinning non-Newtonian fluids in a step-emulsification microdevice. AIChE Journal 68, e17395.
Lobry, E., Theron, F., Gourdon, C., Le Sauze, N., Xuereb, C., Lasuye, T., 2011. Turbulent liquid–liquid dispersion in SMV static mixer at high dispersed phase concentration. Chemical Engineering Science 66, 5762–5774. https://doi.org/10.1016/j.ces.2011.06.073
Meriem-Benziane, M., Abdul-Wahab, S.A., Benaicha, M., Belhadri, M., 2012. Investigating the rheological properties of light crude oil and the characteristics of its emulsions in order to improve pipeline flow. Fuel 95, 97–107. https://doi.org/10.1016/j.fuel.2011.10.007
Michael, V., Prosser, R., Kowalski, A., 2017. CFD-PBM simulation of dense emulsion flows in a high-shear rotor–stator mixer. Chemical Engineering Research and Design 125, 494–510. https://doi.org/10.1016/j.cherd.2017.08.002
Muschiolik, G., Dickinson, E., 2017. Double Emulsions Relevant to Food Systems: Preparation, Stability, and Applications. Comprehensive Reviews in Food Science and Food Safety 16, 532–555. https://doi.org/10.1111/1541-4337.12261
Okazaki, S., Imai, M., Shimizu, M., 1992. Leakage Suppressing Oe W/O Emulsion Using High Viscous Solvent, in: Sekine, T. (Ed.), Process Metallurgy, Solvent Extraction 1990, Part B. Elsevier, pp. 1487–1492. https://doi.org/10.1016/B978-0-444-88677-4.50064-7
Pal, R., 2006. Rheology of high internal phase ratio emulsions. Food Hydrocolloids 20, 997–1005. https://doi.org/10.1016/j.foodhyd.2005.12.001
Pal, R., 1996. Effect of droplet size on the rheology of emulsions. AIChE Journal 42, 3181–3190. https://doi.org/10.1002/aic.690421119

Piorkowski, D.T., McClements, D.J., 2014. Beverage emulsions: Recent developments in formulation, production, and applications. Food Hydrocolloids, Special Issue: A Festschrift in honour of Professor Eric Dickinson 42, 5–41. https://doi.org/10.1016/j.foodhyd.2013.07.009

Raikar, N.B., Bhatia, S.R., Malone, M.F., Henson, M.A., 2009. Experimental studies and population balance equation models for breakage prediction of emulsion drop size distributions. Chemical Engineering Science 64, 2433–2447.

Ramkrishna, D., Singh, M.R., 2014. Population Balance Modeling: Current Status and Future Prospects. Annual Review of Chemical and Biomolecular Engineering 5, 123–146. https://doi.org/10.1146/annurev-chembioeng-060713-040241

Rosti, M.E., Takagi, S., 2021. Shear-thinning and shear-thickening emulsions in shear flows. Physics of Fluids 33, 083319. https://doi.org/10.1063/5.0063180

Sawford, B.L., Hunt, J.C.R., 1986. Effects of turbulence structure, molecular diffusion and source size on scalar fluctuations in homogeneous turbulence. Journal of Fluid Mechanics 165, 373–400. https://doi.org/10.1017/S0022112086003142

Schuch, A., Deiters, P., Henne, J., Köhler, K., Schuchmann, H.P., 2013. Production of W/O/W (water-in-oil-in-water) multiple emulsions: droplet breakup and release of water. Journal of Colloid and Interface Science 402, 157–164. https://doi.org/10.1016/j.jcis.2013.03.066

Skelland, A.H.P., Moeti, L.T., 1989. Effects of surface active agents on minimum impeller speeds for liquid-liquid dispersion in baffled vessels. Ind. Eng. Chem. Res. 28, 122–127. https://doi.org/10.1021/ie00085a021

Theron, F., Le Sauze, N., 2011. Comparison between three static mixers for emulsification in turbulent flow. International Journal of Multiphase Flow 37, 488–500.

Wong, V.-L., Loizou, K., Lau, P.-L., Graham, R.S., Hewakandamby, B.N., 2019. Characterizing droplet breakup rates of shear-thinning dispersed phase in microreactors. Chemical Engineering Research and Design 144, 370–385. https://doi.org/10.1016/j.cherd.2019.02.024

Wong, V.-L., Loizou, K., Lau, P.-L., Graham, R.S., Hewakandamby, B.N., 2017. Numerical studies of shear-thinning droplet formation in a microfluidic T-junction using two-phase level-SET method. Chemical Engineering Science 174, 157–173. https://doi.org/10.1016/j.ces.2017.08.027

Yang, Y., McClements, D.J., 2013. Encapsulation of vitamin E in edible emulsions fabricated using a natural surfactant. Food Hydrocolloids 30, 712–720. https://doi.org/10.1016/j.foodhyd.2012.09.003

Zainal Abidin, M.I.I., Abdul Raman, A.A., Mohamad Nor, M.I., 2014. Experimental Investigations in Liquid–Liquid Dispersion System: Effects of Dispersed Phase Viscosity and Impeller Speed. Ind. Eng. Chem. Res. 53, 6554–6561. https://doi.org/10.1021/ie5002845